

Environmental extreme risk modeling via sub-sampling block maxima

Tuoyuan Cheng ^{1*}, Xiao Peng ², Achmad Choiruddin ³,
Xiaogang He ², Kan Chen ^{1,4}

^{1*} Risk Management Institute, National University of Singapore,
Singapore, 119244, Singapore .

² Department of Civil and Environmental Engineering, National
University of Singapore, Singapore, 117576, Singapore .

³ Department of Statistics, Institut Teknologi Sepuluh Nopember,
Surabaya, 60111, Indonesia .

⁴ Department of Mathematics, National University of Singapore,
Singapore, 119076, Singapore .

*Corresponding author(s). E-mail(s): tuoyuan.cheng@nus.edu.sg;
Contributing authors: xp53@nus.edu.sg; choiruddin@its.ac.id;
hexg@nus.edu.sg; kan.chen@nus.edu.sg;

Abstract

This paper introduces a novel sub-sampling block maxima technique to model and characterize environmental extreme risks. We examine the relationships between block size and block maxima statistics derived from the Gaussian and generalized Pareto distributions. We introduce a weighted least square estimator for extreme value index (EVI) and evaluate its performance using simulated auto-correlated data. We employ the second moment of block maxima for plateau finding in EVI and extremal index (EI) estimation, and present the effect of EI on Kullback-Leibler divergence. The applicability of this approach is demonstrated across diverse environmental datasets, including meteorite landing mass, earthquake energy release, solar activity, and variations in Greenland's land snow cover and sea ice extent. Our method provides a sample-efficient framework, robust to temporal dependencies, that delivers actionable environmental extreme risk measures across different timescales. With its flexibility, sample efficiency, and limited reliance on subjective tuning, this approach emerges as a useful tool for environmental extreme risk assessment and management.

Keywords: block maxima, extremal index, extreme value index, most probable maximum risk, expected maximum risk

MSC Classification: 62P12

1 Introduction

Environmental phenomena—from the sudden, devastating impact of meteorites and colossal energy releases during earthquakes to periodic shifts in solar activity and annual melt events in Greenland’s snow cover and sea ice—pose significant challenges for risk assessment and management. These events, while seemingly disparate, can be analyzed by aggregating or averaging large numbers of random variables (McElreath, 2020). The [central limit theorem \(CLT\)](#) suggests that the sum of many independently distributed random variables, none of which dominates, tends to approximate a Gaussian distribution (Tao, 2012). The [CLT](#) lends credence to beliefs that extreme events are unpredictable outliers, encapsulated in the adage “Natura non facit saltus” (nature does not make jumps) and echoed by “We will never be able to anticipate all discontinuities in financial markets” (Greenspan, 2008; Longin, 2016). However, the [CLT](#) relies on key assumptions, including independence and finite variance. Even when the second moment exists, convergence to a Gaussian is influenced by the existence of higher moments and the heaviness of tails (Kratz, 2016). When these conditions are not met, the Gaussian approximation falls short, prompting the use of power-law models that preserve their functional form under operations such as taking maxima, products, and sums (Gabaix, 2009). Power laws, being scale-invariant, are particularly suited for quantifying extremes and associated environmental extreme risks (de Area Leão Pereira et al., 2017). In this context, [extreme value theory \(EVT\)](#)—grounded in the Fisher-Tippett-Gnedenko and Pickands-Balkema-de Haan theorems—provides specialized asymptotic techniques for estimating parameters, extrapolating high quantiles, and computing tail probabilities, thereby addressing the [CLT](#)’s limitations in modeling environmental extremes (Davison and Huser, 2015).

Within [EVT](#), three parameters are central: the [extreme value index \(EVI\)](#), the [extremal index \(EI\)](#), and the [tail dependence coefficient \(TDC\)](#) (de Haan et al., 2015). The [EVI](#) ξ (the reciprocal of the tail index) characterizes the connection between the magnitudes and frequencies of extremes. The changes in [EVI](#), rather than the average behavior of a random variable, can yield catastrophic outcomes with substantial loss of life and extensive infrastructure damage. The [EI](#) θ represents the reciprocal of the mean duration of extreme clusters (time spent above a threshold, or sojourn time), and describes the recurrence (stickiness) around unstable fixed points in dynamical systems (Moloney et al., 2019). Temporal clustering, evidenced by repeated exceedances of high thresholds, is a prominent feature of extreme events as well as a critical factor in environmental risk modeling (Belzile et al., 2023). The [TDC](#) λ quantifies the dependence between concurrent extremes, regardless of their individual marginal behaviors. The absence of correlation does not imply tail

independence, and vice versa (Sohkanen, 2021). For instance, adjacent river basins may show weak correlation in daily water levels, yet both could experience significant simultaneous flooding during a massive storm. Two cities in the same region share similar climate drivers but may have only one facing a typhoon directly at one time (Huser and Wadsworth, 2022). Collectively, these key parameters capture the scaling, clustering, and tail dependence that define the behavior of environmental extremes, providing the quantitative framework that underpins risk assessment approaches.

Extreme value analysis focuses on the tail of a distribution where the theoretical asymptotics apply for **EVI**, **EI**, and **TDC**. However, because extremes are, by definition, rare, conventional approaches typically discard a large fraction of the data. To accentuate the tail region, the **peaks over threshold (POT)** approach as used in the classical Hill estimator (Hill, 1975) sets a predefined threshold beyond which observations are classified as extreme. Over higher thresholds, exceedances are more likely to be isolated, making the **independent and identically distributed (i.i.d.)** assumption in **maximum likelihood estimator (MLE)** more reliable. However, this comes at the cost of reduced sample sizes for modeling (Moloney et al., 2019). The **MLE** is sensitive to model misspecification, particularly when the **i.i.d.** assumption is violated, and can become unstable in small sample sizes, leading to increased variance in estimates. Additionally, the **POT** approach presents challenges in selecting an appropriate threshold and in handling data censoring (Leadbetter et al., 1983)

While considerable theoretical research has focused on the **POT** method, the **block maxima (BM)** method has garnered less attention (Ferreira and de Haan, 2015). The **BM** approach selects the maximum value from each disjoint block of observations, making it preferable when observations are not strictly **i.i.d.** Under standard mixing conditions, which limit long-range dependence for large values, it has been shown that any two exceedances above large thresholds at sufficiently distant time points become asymptotically independent (Ferreira, 2023). Under mild conditions (Leadbetter et al., 1983), short-term temporal dependence affects only the location and scale parameters of contiguous blocks maxima from stationary processes, while the same shape parameter **EVI** remains consistent for both dependent and independent data. In other words, block maxima preserves asymptotic independence in the presence of temporal clustering. However, the analysis of disjoint **BM** does not account for the clustering of rare events (Davison and Huser, 2015). From a sample efficiency perspective, relying solely on maxima from disjoint blocks may underutilize available data, as other top observations, such as the second-largest values within the blocks, can also provide valuable information.

Historically, extremes were once considered abnormal outliers and discarded before modeling (Longin, 2016). On the contrary in **POT** and **BM**, the vast majority of observations are taken as “below-threshold” or “non-maxima” and similarly discarded. By imposing either a threshold level or a block size, both ways involve subjective censorship of valuable data. **EVT** is inherently data-intensive, as it requires the tail to speak for itself (Nolde and Zhou, 2021). While many proposed parameter estimators

are asymptotically consistent, they may fall short of approaching theoretical values when applied to real-world datasets with limited sample sizes (Clauset et al., 2009; Qu et al., 2022). Moreover, measurement limitations often result in tied observations, creating staircase-style quantile plots and increased uncertainty in estimates. To enhance sample efficiency and fully utilize available data, resampling techniques come into play. However, bootstrap sampling has notable limitations when dealing with small sample sizes, non-finite variances, or dependence structures (Chernick and NetLibrary, 2008). In contrast, sub-sampling (resample without replacement) generates masked subsets of real observations, where all observations have opportunities to be resampled, dependence structure is preserved, and heavy tails can be processed (Politis et al., 1999).

Recent research underscores the importance of EVT in modeling environmental extreme risks (Davison and Huser, 2015; Gabaix, 2016). In environmental science, EVT-based models help to detect anthropogenic influences on temporal extremes and contribute to our understanding of climate change impacts (Zwiers et al., 2013). Human societies face constant exposure to environmental extremes, making the statistical analysis of these events promising for predicting their effects and implementing mitigation strategies (Smith and Katz, 2013). Practical applications of EVT include analyzing the dynamics of natural disaster-linked insurance policies (Smolka, 2006) and assessing catastrophe bonds (Nadarajah et al., 2018).

The quest for a unified best practice methodology to model univariate environmental extremes in the presence of complex trends remains a critical challenge (Clarkson et al., 2023). To address this, we propose a sub-sampling block maxima approach for constructing and characterizing univariate risk measures. This approach produces U-statistics that are permutation invariant, asymptotically Gaussian (Jochem Oorschot et al., 2023), and possess infinitely differentiable sample paths (Wager, 2014), rendering them less sensitive to the choice of block size (Belzile et al., 2023). To illustrate this methodology, we introduce the most probable maximum risk (MPMR) alongside the expected maximum risk (EMR) and establish their connections to the EVI. We introduce a weighted least square estimator (WLSE) for EVI and evaluate its performance using simulated auto-correlated data. We employ the second moment of BM for plateau finding in EVI and EI estimation, and present the effect of EI on Kullback–Leibler divergence (KLD). We demonstrate the utility of this approach on diverse datasets covering natural hazards and climate variations, thereby offering practitioners a sample-efficient, flexible, and objective tool for modeling environmental extreme risks.

2 Block maximum, expected maximum risk, and most probable maximum risk

We begin by examining the distribution of block maxima. For a block of size n sampled from i.i.d. random variables with a distribution function $F_X(\cdot)$ belonging to the maximum domain of attraction (MDA) of Frechet or Gumbel (i.e. $F_X \in MDA_\xi$, $\xi \geq 0$)

and a density function $f_X(\cdot)$, the maximum of the block (BM) M has the following distribution function and density function (Bouchaud and Potters, 2003; Chen and Cheng, 2022):

$$\begin{aligned} F_M(m) &= (F_X(m))^n \\ f_M(m) &= \frac{\partial (F_X(m))^n}{\partial m} = n f_X(m) (F_X(m))^{n-1} \end{aligned} \quad (1)$$

The MPMR m^* is defined as the mode of M , determined by solving:

$$\begin{aligned} \left. \frac{\partial f_M(m)}{\partial m} \right|_{m=m^*} &= 0 \\ \left[\frac{\partial f_X(m)}{\partial m} (F_X(m))^{n-1} + f_X(m) (n-1) (F_X(m))^{n-2} f_X(m) \right] \Big|_{m=m^*} &= 0 \\ \left[\frac{\partial f_X(m)}{\partial m} F_X(m) + (n-1) f_X^2(m) \right] \Big|_{m=m^*} &= 0 \end{aligned} \quad (2)$$

Asymptotically as $n \rightarrow \infty$ and $F_X(m) \rightarrow 1$, we have:

$$\left[\frac{\partial f_X(m)}{\partial m} + n f_X^2(m) \right] \Big|_{m=m^*} = 0 \quad (3)$$

Both Eqs. (2) and (3) can be solved numerically using root-finding algorithms (Oliveira and Takahashi, 2020).

The KLD between M and X quantifies their dissimilarity in terms of block size n :

$$D_{KL}(M\|X) = \int \log \left(\frac{f_M(t)}{f_X(t)} \right) f_M(t) dt = \frac{1}{n} + \log(n) - 1 \quad (4)$$

$$D_{KL}(X\|M) = \int \log \left(\frac{f_X(t)}{f_M(t)} \right) f_X(t) dt = n - \log(n) - 1 \quad (5)$$

To maintain conciseness, the relationship between MPMR m^* and block size n , assuming several well-known underlying distributions for $f_X(\cdot)$ is provided in Appendix A. In some cases, the EMR (denoted $\bar{m} = \mathbb{E}[M]$) is also shown.

In particular, for a fat-tailed random variable $Y \sim GPD(\frac{1}{\xi}, 1, \xi)$, $\xi > 0$ in the MDA of Frechet, the transformation $X = \log(\xi Y) \sim Exp(\frac{1}{\xi})$ places it in the MDA of Gumbel. Using X , the linear relationship between its MPMR/EMR and $\log(n)$ (see

Table 1 Cumulative distribution function of the **BM** distribution given exponential underlying, evaluated around the **MPMR**, keeping the leading order term when the block size $n \rightarrow \infty$.

k	$\lim_{n \rightarrow \infty} F_M \left(m^* + k \frac{\xi \pi}{\sqrt{6}} \right)$	value
-3	$e^{-e^{-\sqrt{\frac{3}{2}} \pi}}$	4.35599×10^{-21}
-2	$e^{-e^{-\sqrt{\frac{2}{3}} \pi}}$	2.25592×10^{-6}
-1	$e^{-e^{-\frac{\pi}{\sqrt{6}}}}$	0.0271651
0	$\frac{1}{e}$	0.367879
1	$e^{-e^{-\frac{\pi}{\sqrt{6}}}}$	0.757805
2	$e^{-e^{-\sqrt{\frac{2}{3}} \pi}}$	0.925972
3	$e^{-e^{-\sqrt{\frac{3}{2}} \pi}}$	0.978896

Eqs. (A1) and (A2) allows for estimation of the **EVI** parameter ξ of Y via least-square. Moreover, the **BM** of X has its infinite order moments exist, among which its variance remains constant and independent of subsample size n (see Eq. (A3)). Using Eq. (A4), the distribution function of the **BM** around the **MPMR** of X is evaluated and tabulated in Table 1. The **BM** distribution is heavily right-skewed, with over 92.59% of its density concentrated below $m^* + 2\frac{\xi \pi}{\sqrt{6}}$. Consequently, m^* is suitable for estimating ξ , and $m^* + 2\frac{\xi \pi}{\sqrt{6}}$ can serve as a practical threshold for managing extreme environmental risks.

3 Sub-sampling block maximum and weighted least square estimator for extreme value index

In this section, assuming **generalized Pareto distribution (GPD)** as the underlying distribution, we discuss the estimation of **MPMR/EMR** and present the **WLSE** estimation of **EVI**.

3.1 Estimating **MPMR** and **EMR** by weighted average

We start with a raw sample x of size N , where $x_{[i]}$, $i = 1, \dots, N$ represents the i -th smallest value in the raw sample x . For a sub-sample of size n , the **BM** M_n is selected from the top $N - n + 1$ elements in x . The probability $p_{n,i} = \mathbb{P}(M_n = x_{[i]})$ of choosing the i -th value as the **BM**, with the remaining $n - 1$ values drawn from those smaller than it, is given by:

$$\begin{aligned}
 p_{n,i} &= \frac{\binom{i-1}{n-1}}{\sum_{j=n}^N \binom{j-1}{n-1}}, \quad i = n, \dots, N \\
 &= \frac{\binom{i-1}{n-1}}{\binom{N}{n}} \tag{6}
 \end{aligned}$$

Using this probability, the **EMR** can be estimated as $\widehat{m}_n = \sum_{i=n}^N p_{n,i} x_{[i]}$, and other moments can be sequentially computed using online algorithms (Welford, 1962).

The **MPMR** \widehat{m}_n^* is estimated non-parametrically using the mean-shift algorithm with Gaussian kernels and Scott bandwidth (Cheng, 1995; Aliyari Ghassabeh, 2013), which also leads to a weighted average.

Both \widehat{m}_n and \widehat{m}_n^* are U-statistics that are permutation invariant, asymptotically Gaussian with variance decaying as $\frac{1}{n}$ (Jochem Oorschot et al., 2023). They are smooth with respect to (w.r.t.) n (Wager, 2014), making them robust to block size selection (Belzile et al., 2023). The proposed risk measure (**MPMR** or **EMR**) estimates use the full sample, thereby achieving high sample efficiency.

At all block sizes n , the element with the largest $p_{n,i}$ in Eq. (6) is always $x_{[N]}$. At a small block size n , **MPMR** predominantly captures the central portion of the distribution; as n increases, **MPMR** gradually accentuates the tail part of the distribution. When n approaches the raw sample size N , the finite sample effect becomes pronounced since \widehat{m}_n^* is constrained by $x_{[N]}$ and the variance of the estimate shrinks towards 0. Consequently, the estimation of \widehat{m}_n^* for sufficiently large n requires extrapolation using the **EVI** ξ .

3.2 Estimating **EVI** by **WLSE**

Following Section 2, the **EVI** ξ can be estimated using least square regression, based on the linear relationships $\widehat{m}_n^* \sim \log(n)$ and $\widehat{m}_n \sim \sum_{i=1}^n \frac{1}{i}$ for samples from a **GPD** in the **MDA** of Frechet (see Eqs. (A1) and (A2)). Prior to this estimation, a log transformation is applied to map observations from the **MDA** of Frechet to that of Gumbel, facilitating computation of **MPMR** and **EMR** estimates.

Since the sequences $\log(n)$ and $\sum_{i=1}^n \frac{1}{i}$ become tightly clustered as n increases, a **WLSE** is preferred. For \widehat{m}_n^* , the weight at a given n is $w_n = \frac{\partial \log(n)}{\partial n} = \frac{1}{n}$. For \widehat{m}_n , the weight at a given n is $w_n = \frac{\partial \sum_{i=1}^n \frac{1}{i}}{\partial n} = \frac{\pi^2}{6} - \sum_{i=1}^n \frac{1}{i^2} \approx \frac{1}{n+1}$. Alternatively, computation can be accelerated by evaluating \widehat{m}_n^* and \widehat{m}_n at geometrically spaced n , providing asymptotically equivalent results.

At every n , both $\frac{\partial \widehat{m}_n^*}{\partial \log(n)}$ and $\frac{\partial \widehat{m}_n}{\partial \log(n)}$ offer estimates of ξ . To avoid subjectivity (Wager, 2014), ξ is calculated over a range of n , excluding small n , where **EMR/MPMR** does not adequately reflect extreme behaviors, and large n , where finite sample effects dominate. The ideal n regime, where the variance of **BM** is independent of n , as shown in Eq. (A3), guides the selection of this range. A suitable range of n is determined by identifying a plateau in the standard deviation spline $g(n) := \sqrt{\mathbb{V}[M_n]}$ using the following criteria:

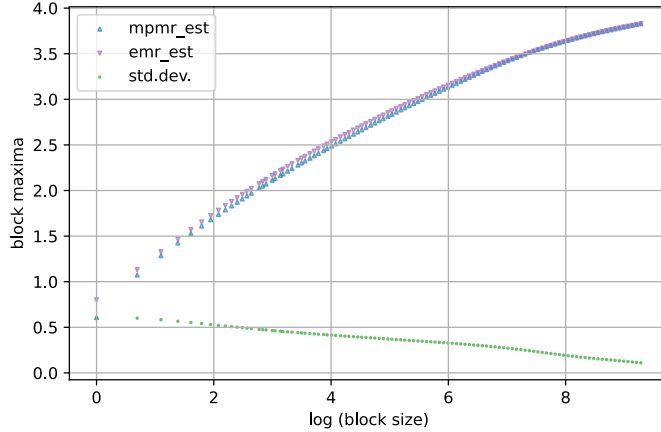


Fig. 1 Dependence of **MPMR**, **EMR**, and **BM** standard deviation on block size n , using simulated *i.i.d.* half-Gaussian observations.

$$\begin{aligned}
 n^* &= \arg \min_n \left\{ \frac{\partial g}{\partial \log(n)} \right\}^2 \\
 n_{\min} &= g^{-1}((1 + \Delta) g(n^*)) \\
 n_{\max} &= g^{-1}((1 - \Delta) g(n^*))
 \end{aligned}$$

where Δ is a hyper-parameter, typically set to 0.1. The search for n^* usually begins at $n_0 = \sqrt{N}$. Least-square estimates of ξ are then calculated using the range $n \in [n_{\min}, n_{\max}]$.

3.3 Simulation

3.3.1 Dependence of **MPMR** and **EMR** on block size

In this section, we analyze the behavior of **MPMR** and **EMR** using simulated *i.i.d.* data drawn from a half-Gaussian distribution and a half-Student- t distribution.

We first consider a half-normal distribution, $X = |Y|$, where Y follows a standard Gaussian distribution. Fig. 1 illustrates the **MPMR**, **EMR**, and **BM** standard deviation estimates based on *i.i.d.* samples from X with a raw sample size of $N = 50000$. In Fig. 1 the vertical axis is in the original scale of X . As $\log(n)$ increases, both **MPMR** and **EMR** estimates rise with diminishing tangent slopes, while the standard deviation estimates decrease continuously without exhibiting a plateau, indicating that the underlying distribution is less extreme than the exponential distribution.

Next, we consider $X = \log(|Y|)$, with Y following a Student's t distribution with a degree of freedom $\nu = 3$. The Student's t has its tail in the **MDA** of Fréchet with

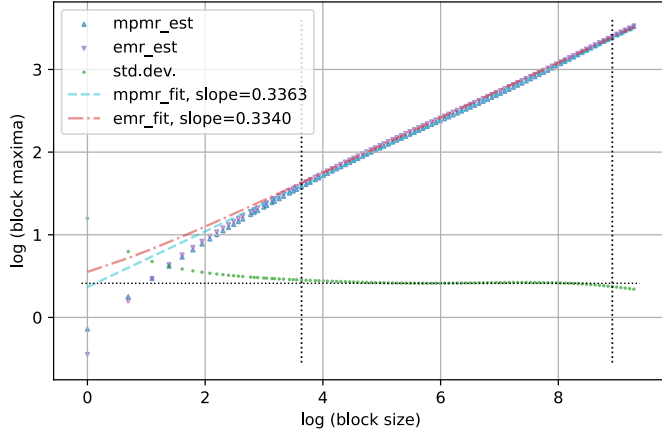


Fig. 2 Dependence of **MPMR**, **EMR**, and **BM** standard deviation on block size n , using simulated **i.i.d.** half-Student's t observations, with the degree of freedom $\nu = 3$, theoretical $\xi = \frac{1}{3}$.

a theoretical **EVI** $\xi = \frac{1}{\nu}$. Fig. 2 displays the **MPMR**, **EMR**, and the **BM** standard deviation estimates together with selected n_{\min}, n_{\max} and the fitted lines, based on **i.i.d.** samples from X with a raw sample size of $N = 50000$. In Fig. 2 the vertical axis is in the log scale of $|Y|$. Both **MPMR** and **EMR** sequences exhibit evident scaling (as shown in this log-log plot) within the range of n , as indicated by the plateau of **BM** standard deviation. The **WLSE** provides **EVI** estimates close to $\frac{1}{3}$.

3.3.2 Estimator performances

In this section, we evaluate the performance of the proposed **EVI** estimators using data sampled from $Y_i = \exp(X_i)$, where $X_i = \phi X_{i-1} + \epsilon_i$, $\epsilon_i \sim \text{Exp}(\frac{1}{\xi})$, $\phi \in \{0, 0.1, 0.5, 0.9\}$, $\xi \in [0.1, 10]$, $i \in \{1, \dots, 365\}$. The theoretical **EVI** of Y_i remains constant at ξ (Gabaix, 2009). This design incorporates both extremes and serial correlations, resembling real-world data scenarios.

Using samples of 365 observations, we apply the proposed **EMR/MPMR-WLSE** estimators from Section 3.2 on log-transformed data. For benchmarking, we included Hill's estimator (Hill, 1975), Meerschaert and Scheffler's estimator (Meerschaert and Scheffler, 1998), Schultze and Steinebach's estimator (Schultze and Steinebach, 1996), and Smith's estimator (Smith, 1987), which have been reported among the best-performing estimators in a comparative review of over 90 estimators (Fedotenkov, 2020). Performances are summarized using the **mean absolute percentage error (MAPE)**, averaged among 666 samples generated with different random seeds.

Results are shown in Fig. 3, presented on a log scale for enhanced visibility. For $\phi \in \{0, 0.1\}$, Schultze and Steinebach's estimator consistently achieved the lowest **MAPE** across $\xi \in [0.1, 10]$. At $\phi = 0.9$, Hill's and the Smith's estimators demonstrated

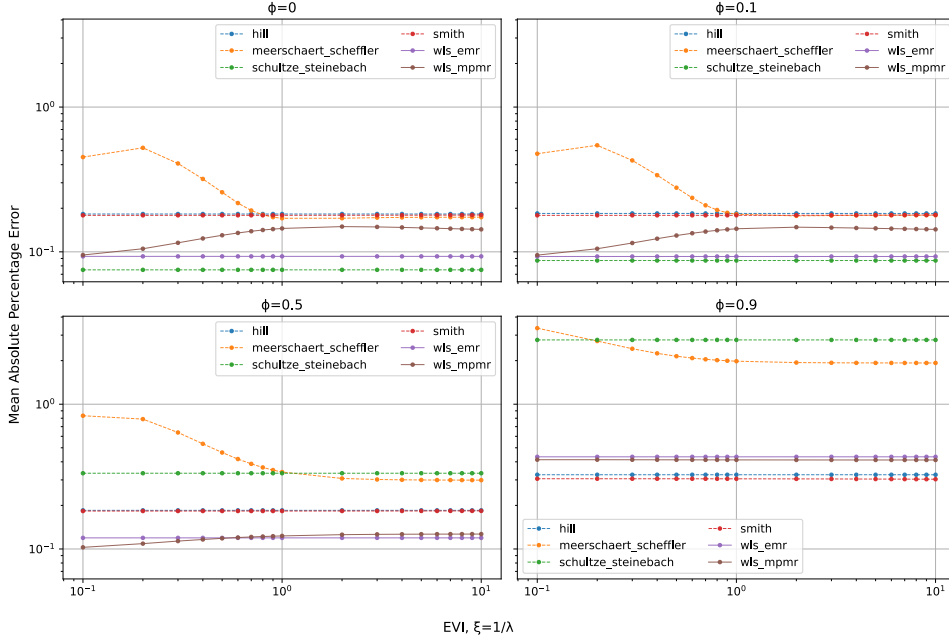


Fig. 3 Mean absolute percentage error **MAPE** of different **EVI** estimators across various autocorrelation levels (ϕ) along increasing theoretical **EVI** values (ξ , shown on log scale), using data sampled from $Y_i = \exp(X_i)$, where $X_i = \phi X_{i-1} + \epsilon_i$, $\epsilon_i \sim \text{Exp}(\lambda = \frac{1}{\xi})$, $\phi \in \{0, 0.1, 0.5, 0.9\}$, $\xi \in [0.1, 10]$, $i \in \{1, \dots, 365\}$.

superior performance. The proposed **EMR/MPMR-WLSE** estimators exhibited balanced performances for $\xi \in [0.1, 10]$, achieving the lowest **MAPE** when $\phi = 0.5$.

Overall, the proposed **EMR-WLSE** estimator demonstrated robustness across varying levels of autocorrelation (ϕ) and theoretical **EVI** (ξ), maintaining consistently low **MAPE** values. Additionally, the scalability along $\log(n)$, as discussed in Section 3.3.1, offers visual interpretability, a key advantage over traditional methods.

3.4 Meteorite landing impact risk

Now we turn to an example of empirical data analysis using our method. Meteorite landings are known extraterrestrial impact risks with the potential to cause mass extinctions. The kinetic energy generated upon impact is directly proportional to the mass of the meteorite, and only meteorites exceeding a certain mass threshold survive their passage through Earth's atmosphere. While multiple meteorites might originate from the same near-Earth object, their impacts can generally be treated as **i.i.d.** when assessing risk due to the independence of individual landings.

In Fig. 4, we analyze meteorite landing mass records obtained from NASA and the Meteoritical Society (Gattacceca et al., 2023) to explore the scaling properties of these events. The dataset, comprising $N = 42465$ observations, was analyzed using

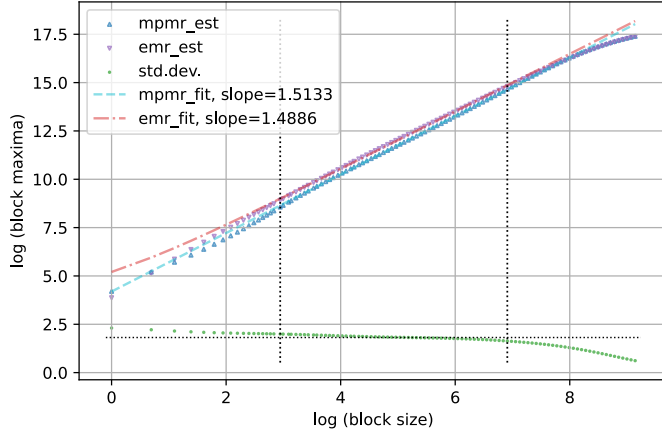


Fig. 4 Dependence of **MPMR**, **EMR**, and **BM** standard deviation on block size n , based on meteorite landing mass (in grams).

the **WLSE** method on log-transformed masses. The vertical axis in Fig. 4 represents the log-scale of the meteorite landing masses (in grams).

The results show that the **WLSE** provides an estimated $\hat{\xi} \approx 1.50 > 1$. By definition, a $\xi > 1$ implies that the original (untransformed) distribution has a very heavy tail such that its **EMR** does not exist. This finding supports the widely held understanding that, while catastrophic meteorite impacts are rare, they pose significant risks over geological timescales. This result highlights the importance of ongoing monitoring and preparedness for mitigating potential meteorite impact risks. Future research could extend this assessment by incorporating near-Earth objects to provide a more comprehensive risk evaluation.

4 Clustering of extremes

Rather than being **i.i.d.**, extremes often exhibit temporal clustering, which can be quantified by the **EI**. Let $\mathbf{X} = \{X_n\}_{n \geq 1}$ represent a stationary sequence of random variables with a common marginal distribution function $F_X(\cdot)$. The sequence $\{\mathbf{X}\}$ is said to have an **EI**, denoted by $\theta \in (0, 1]$, if for each $\tau > 0$ there exists a sequence of normalized levels u_n , such that $n(1 - F_X(u_n)) \rightarrow \tau$ as $n \rightarrow \infty$, and $\mathbb{P}(M_n \leq u_n) \rightarrow \exp(-\theta\tau)$, where M_n is the **BM** of a consecutive block. When $\theta = 1$, the tail behavior of \mathbf{X} resembles an **i.i.d.** sequence, whenever $\theta < 1$ leads to clusters of extreme values (Ferreira, 2023). This definition uses approximations from binomial to Poisson distributions and assumes an exponential distribution function when the number of exceedances $n_u = 0$. Additionally, $n(1 - F_X(M_n)) \sim \text{Exp}(\theta)$ and approximately $-n \log(F_X(M_n)) \sim \text{Exp}(\theta)$. These relationships enable the use of sample moments as estimators for θ (Berghaus and Bücher, 2018; Northrop, 2015).

Using the above definition, the **KLD** can be expressed as:

$$\begin{aligned}
D_{KL}(M_n \| X) &= \int \log \left(\frac{f_{M_n}(t)}{f_X(t)} \right) f_{M_n}(t) dt &&= \mathbb{E}^{M_n} \left[\log \left(\frac{f_{M_n}}{f_X} \right) \right] \\
&= \frac{1}{n\theta} + \log(n\theta) - 1 && \tag{7}
\end{aligned}$$

$$\begin{aligned}
D_{KL}(X \| M_n) &= \int \log \left(\frac{f_X(t)}{f_{M_n}(t)} \right) f_X(t) dt &&= \mathbb{E}^X \left[\log \left(\frac{f_X}{f_{M_n}} \right) \right] \\
&= n\theta - \log(n\theta) - 1 && \tag{8}
\end{aligned}$$

By comparing Eqs. (7) and (8) with Eqs. (4) and (5), we can interpret that **EI** describes clustering by quantifying the loss of **i.i.d.** degrees of freedom (Moloney et al., 2019). With **EI**, the previous **MPMR** and **EMR** equations in Section 2 and Section 3 will have n substituted by $n\theta$, but the **EVI** estimators are not affected. The mean duration of extreme clusters (i.e., time spent above a threshold, or sojourn time) is quantified as $\frac{1}{\theta}$. The **EI** also captures the recurrences around unstable fixed points (“stickiness”) in dynamical systems (Moloney et al., 2019).

4.1 Estimating **EI** by block maxima

To estimate the **EI**, rolling windows (temporal consecutive sliding blocks) of block size n are applied to the raw \mathbf{X} time series, generating a sequence of resampled **BM**. The resampled **BMs** are used to compute either $Z_{n,\text{BB}} = n (1 - F_X(M_n))$ or $Z_{n,\text{Northrop}} = -n \log(F_X(M_n))$. Both of them follow an exponential distribution parameterized by θ with a mean of $\frac{1}{\theta}$ and variance of $\frac{1}{\theta^2}$. The reciprocal of the average of $Z_{n,\text{BB}}$ or $Z_{n,\text{Northrop}}$ at each n provides an estimate of θ .

At small n , the re-sampled values of $1 - F_X(M_n)$ or $-\log(F_X(M_n))$ exhibit large standard deviations. However, the Z_n estimates and their standard deviations remain small due to the small block size n . Conversely, at large n , the re-sampled values of $1 - F_X(M_n)$ or $-\log(F_X(M_n))$ has small values and small standard deviations (goes to zero faster than $1/n$ as $n \rightarrow N$). Consequently, the Z_n estimates typically form a peak plateau over a mid-range of n . Traditionally, researchers identify the **EI** by locating this plateau.

For simplicity, we determine **EI** estimates when the accompanying standard deviations reached its maximum. To balance computational efficiency and smoothness, the rolling window step size for a given n is set to \sqrt{n} . In practice, $\widehat{\theta}_n$ depends on the temporal resolution of the time series. Poorly resolved time series may result in under-resolved clusters, artificially inflating empirical **EI** values. This underscores the importance of appropriate temporal resolution in estimating the **EI**.

4.2 Earthquake energy release risk

Earthquakes pose significant risks to public safety and infrastructure through ground shaking, structural damage, and secondary hazards like landslides and tsunamis.

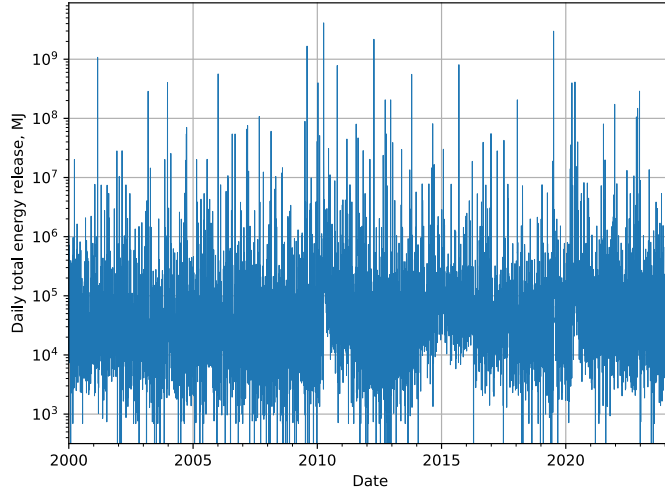


Fig. 5 Time series of daily earthquake energy release (in megajoules) in conterminous U.S. since 2000.

They can strike in clusters within a localized area over a relatively short time frame, often followed by aftershocks. Seismic hazard assessments are critical for informing infrastructure design, land-use planning, and emergency response strategies.

In Fig. 5, the time series of daily total earthquake energy release (measured in megajoules) across the conterminous U.S. since 2000 is plotted using data from the USGS (US Geological Survey, 2017). The dataset includes 8752 daily records of earthquakes with magnitude ≥ 2.12 . After preliminary analysis, the marginal distribution is modeled using a GPD with a log transformation applied before estimating parameters using the WLSE.

Fig. 6 illustrates the dependence of key metrics (MPMR, EMR, and BM standard deviation) on block size n . The vertical axis is displayed on a log scale, revealing a heavy-tailed distribution with an EVI estimate of $\hat{\xi} \approx 1.56 > 1$, indicating evident heavy-tailed behavior, consistent with the high energy release observed in extreme earthquake events.

Fig. 7 charts the reciprocal of EI estimates $\frac{1}{\hat{\theta}}$ across various block size n . The estimated $\frac{1}{\hat{\theta}} \approx 1.23$ suggests relative independence in the record sequences at the daily resolution level for the conterminous U.S. region. Additionally, we have tabulated the earthquake magnitudes corresponding to the quantiles of maximum daily energy release over several years in the conterminous U.S. as in Table 2. These values serve as practical benchmarks for seismic risk assessment and earthquake-resilient infrastructure design.

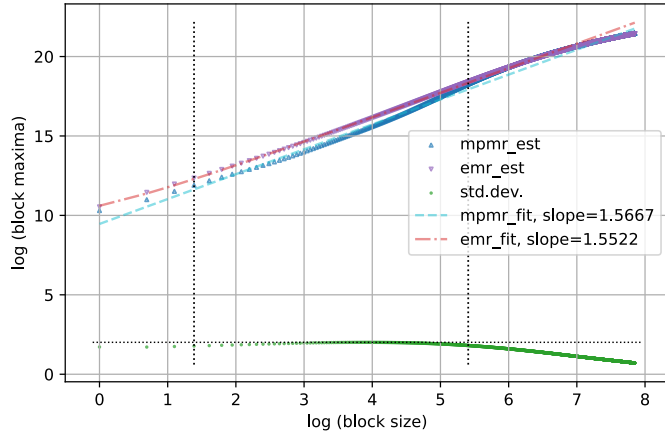


Fig. 6 Dependence of **MPMR**, **EMR**, and **BM** standard deviation on block size n , using daily earthquake energy release (in megajoules) in conterminous U.S.

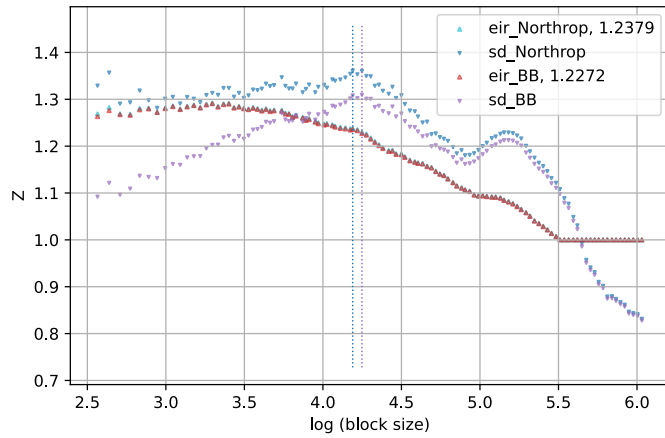


Fig. 7 Reciprocal of **EI** (days) for daily earthquake energy release in conterminous U.S.

Table 2 Earthquake magnitudes corresponding to $m^* + k \frac{\xi\pi}{\sqrt{6}}$, over different time frames, for daily earthquake energy release in conterminous U.S.

		number of years		
		1	10	100
k	0	6.1695	7.2575	8.3455
	1	6.7755	7.8635	8.9516
	2	7.3816	8.4696	9.5576

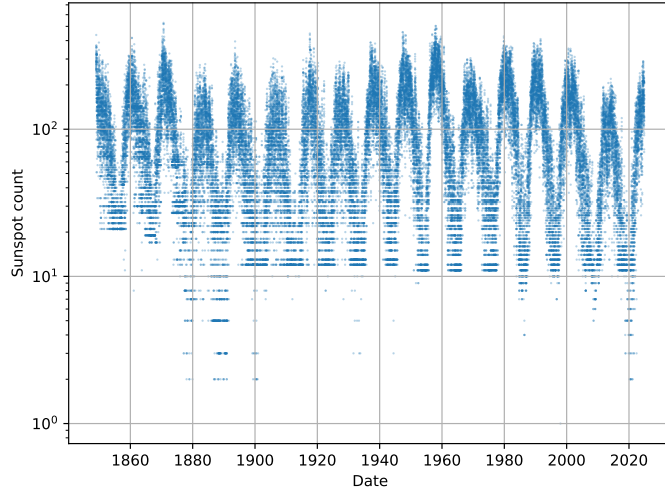


Fig. 8 Daily sunspot counts since 1849.

4.3 Solar activity risk

Solar activity influences space weather near Earth, potentially causing geomagnetic storms that disrupt power grids, communication systems, and navigation systems. It also poses radiation hazards to astronauts and high-altitude polar flights passengers. Some studies suggest a relationship between periods of low solar activity and global cooling, emphasizing the interplay between solar phenomena and terrestrial climate dynamics (Shindell et al., 2001). Understanding the temporal clustering patterns of solar activity can aid in assessing space weather risks and devising mitigation strategies.

Fig. 8 illustrates the time series of daily sunspot counts since 1849, based on records from SILSO (SILSO World Data Center, 1849-2024). Although detailed intensity metrics like flux or irradiance were unavailable in earlier years, this long-term dataset provides rich insights spanning multiple solar cycles. We model the marginal distribution of daily sunspot counts using an exponential distribution such that WLSE is performed without log transform.

Fig. 9 has its vertical axis in the original scale of daily sunspot counts. The results indicate a slope estimate of approximately 38.

Fig. 10 charts the reciprocal of EI estimates, revealing an approximate solar cycle duration of 11 years with peaks clustered over 98 days. These findings provide insights into solar activity clustering, contributing to the understanding of its temporal dynamics and associated risks.

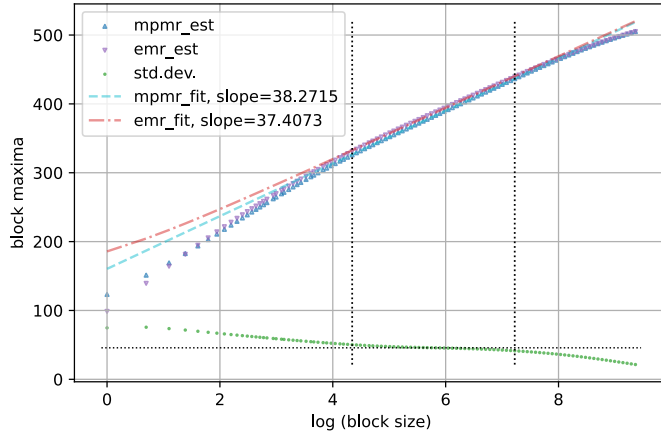


Fig. 9 Dependence of MPMR, EMR, and BM standard deviation on block size n , using daily sunspots.

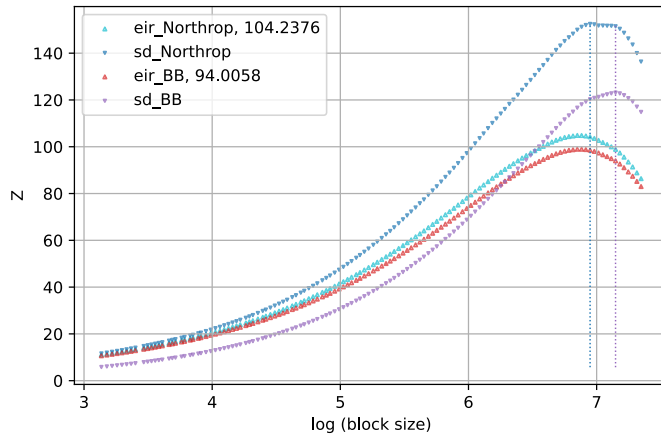


Fig. 10 Reciprocal of EI estimates (days) for daily sunspots.

4.4 Greenland land snow cover melt risk

The Greenland ice sheet, the second-largest ice sheet on Earth, is critical to global climate dynamics. Its melting has profound implications, contributing to rising sea levels, altering ocean salinity, and affecting the Atlantic meridional overturning circulation. These processes can accelerate global warming through feedback loops, impacting both regional ecosystems and global climate patterns.

Fig. 11 depicts the time series of weekly Greenland land snow cover log loss since 1966, based on records from the Rutgers University Global Snow Lab (Estilow et al., 2015). The log loss is calculated as $r_t = \log(\max_T y_T) - \log(y_t)$ where $\max_T y_T$ is the maximum snow cover extent area (in million square kilometers) in the entire

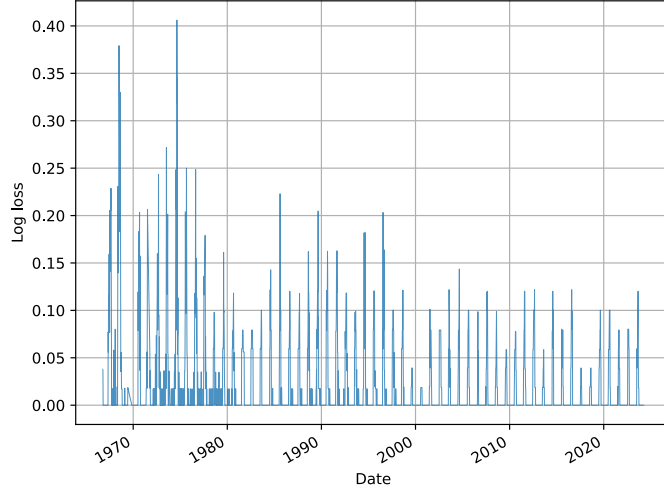


Fig. 11 Time series of weekly Greenland snow cover log loss since 1966.

observation history, and y_t is snow cover extent area at week t . The percentage loss $r_{t,\text{pct}} = \exp(r_t) - 1 \in [0, 1]$ follows a Beta distribution as in the [MDA](#) of Weibull, while the log loss $r_t = \log(1 + r_{t,\text{pct}}) \in [0, \infty)$ enables reuse of the [GPD](#) in the [MDA](#) of Frechet. Following initial modeling, we model the marginal distribution of the log loss sequence in [GPD](#) and apply a log transform on it before [WLSE](#).

Fig. [12](#) has its vertical axis in the log scale of raw log loss sequence. The estimated [EVI](#) $\hat{\xi} \approx 0.23$ indicates moderate tail behavior, consistent with gradual changes observed over time.

Fig. [13](#) charts the reciprocal of [EI](#) estimates, suggesting that Greenland’s annual land snow cover freeze-thaw cycle exhibits clustering with peaks persisting on average for 6 weeks. These findings provide insights into seasonal snow dynamics, emphasizing the need for continued monitoring to assess climate risks associated with Greenland’s ice sheet.

4.5 Greenland sea ice extent melt risk

The Greenland sea ice extent acts as a regulator of the Earth’s climate and is geographically close to the landmass of Greenland. Arctic warming has accelerated the reduction of sea ice extent, amplifying the albedo feedback effect and impacting global climate systems. This decline has also created opportunities for new maritime routes and increased regional shipping activities. Monitoring sea ice extent is essential for understanding climate change impacts and developing mitigation strategies.

Fig. [14](#) depicts the time series of daily Greenland sea ice extent log loss since 1978, based on records from the NSIDC ([Fetterer et al., 2017](#)). The log loss is calculated

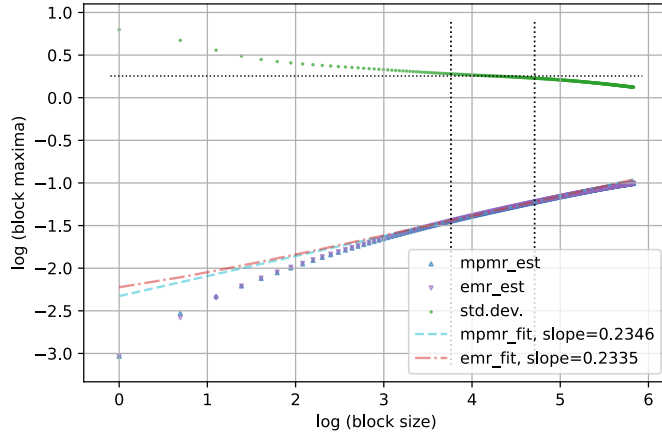


Fig. 12 The dependence of MPMR, EMR, and BM standard deviation on block size n , using weekly Greenland snow cover log loss.

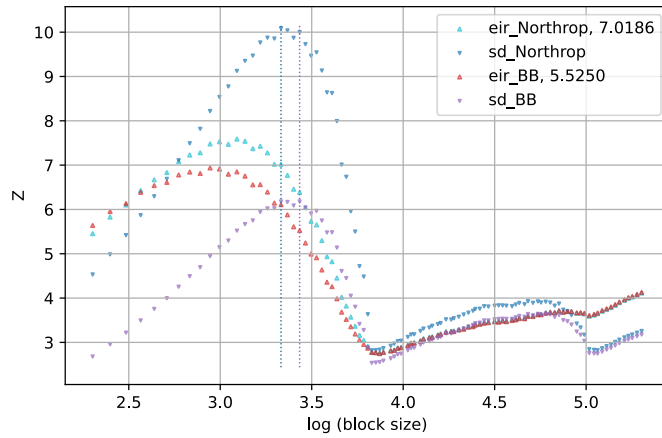


Fig. 13 Reciprocal of EI (weeks) for weekly Greenland snow cover log loss.

using a similar approach as in Section 4.4. We model the marginal distribution of the log loss sequence using a Gaussian distribution, selected for our analysis based on Akaike information criterion.

Fig. 15 has its vertical axis in the original scale of the log loss sequence.

Fig. 16 charts the reciprocal of the EI estimates, indicating that Greenland's annual sea ice extent freeze-thaw cycle has its peaks clustered on average for 42 days, which aligns closely to the annual Greenland land snow cover period estimated in Section 4.4, indicating regional consistency in cryospheric responses to seasonal and climate variations.

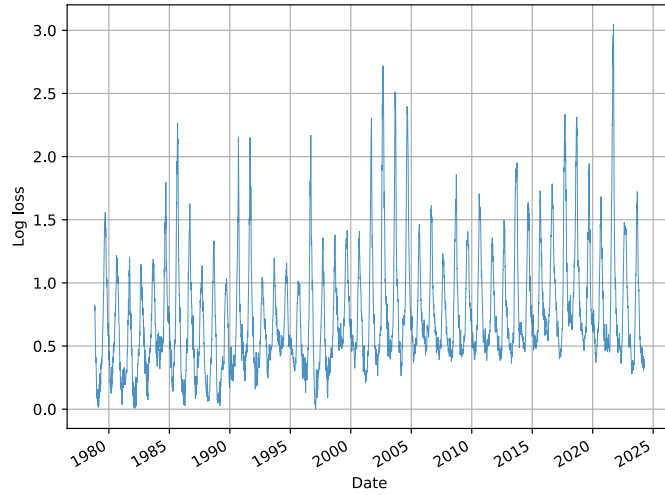


Fig. 14 Time series of daily Greenland sea ice extent log loss since 1978.

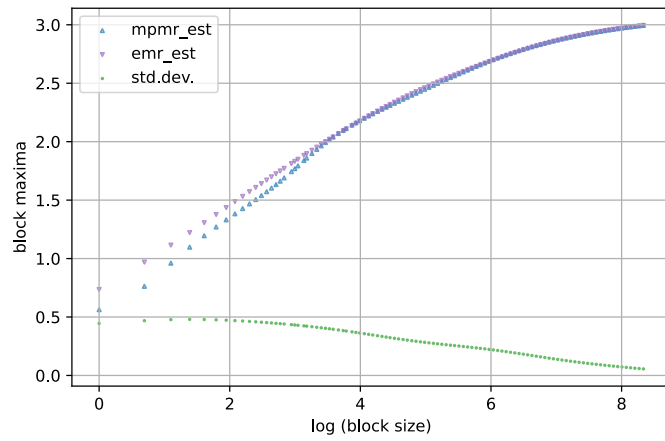


Fig. 15 The dependence of **MPMR**, **EMR**, and **BM** standard deviation on block size n using daily Greenland sea ice extent log loss.

5 Environmental extreme risk modeling: from accustomed to unprecedented

In this section, we outline a flexible and robust procedure for environmental extreme risk modeling using our proposed methodology.

The process begins with the estimation of **MPMR** m^* , as detailed in Section 3.1. This measure is flexible, as $F_M(m^*)$ is asymptotically constant across all considered **MDA** outlined in Appendix A.

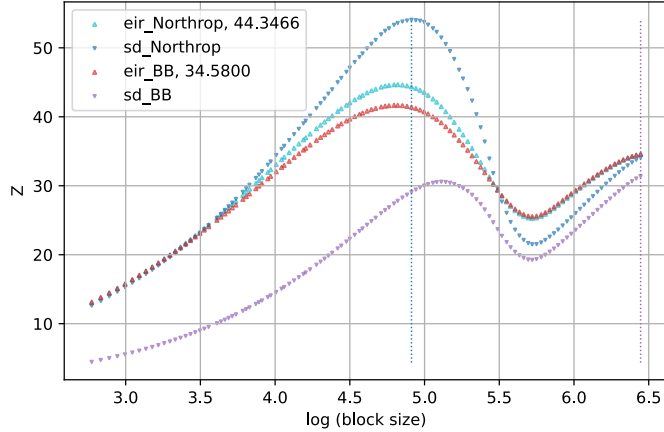


Fig. 16 Reciprocal of **EI** (days) of daily Greenland sea ice extent log loss

Accustomed risks refer to short- to medium-term extreme events where recovery is feasible within practical timescales. For these risks, strategies can be formulated around m_n^* , the **MPMR** calculated for an intermediate level block size n . This approach assumes that the replenishment of recovery resources remains sustainable within these temporal bounds.

Unprecedented risks refer to long-term extreme events. In these cases, an extreme emergency reserve is proposed as $\frac{m_n^*}{\theta}$. This integrates the estimated **EVI** (Section 3.2) for extrapolating **MPMR** at larger block sizes n and adjusts for temporal clustering effects through the **EI** estimate (Section 4.1).

By using **MPMR** and **EI**, this dual-layered approach addresses the temporal distortions often associated with non-i.i.d. extremes. It ensures that risk estimates remain actionable and realistic, even under complex dependencies and clustering phenomena.

6 Conclusions

This paper presents a novel sub-sampling **BM** approach for environmental extreme risk modeling. We explore the relationship between block sizes and the **BM** statistics originating from both Gaussian and **GPDs**, and demonstrate the efficacy of our method using simulated auto-correlated data and real-world environmental extremes. Central to our framework are the concepts of the **MPMR** and temporal clustering quantified by **EI**. This dual-layered approach enhances sample efficiency and reduces the need for subjective identification of non-extreme and tail regions, providing a robust and practical tool for extreme risk assessment and management.

Looking ahead, future research may employ rolling windows to uncover the dynamics of underlying parameters. Our approach, with its enhanced sample efficiency, holds

particular value for regions most vulnerable to climate change, especially in developing or underdeveloped worlds (Nadarajah, 2023). Additionally, Eq. (7) and Eq. (8) suggest the potential for a KLD-based EI estimator.

Declarations

Ethical Approval

Not Applicable

Availability of supporting data

The Python scripts developed for computation and visualization in this research and investigated datasets are accessible via a dedicated GitHub repository <https://github.com/TY-Cheng/UniBM> under the GNU Lesser General Public License Version 3 (LGPL-3.0) license. Researchers and enthusiasts interested in replicating, extending, or exploring our methods and findings are encouraged to visit the repository.

Competing interests

The authors have no competing interests to declare that are relevant to the content of this article.

Funding

This research is partly supported by the Singapore Ministry of Education academic research grant R-144-000-457-733 on Outbreak Resilience, Forecasting, and Early Warning.

Appendix A **MPMR** and block size

In this appendix, we show the relationship between **MPMR** m^* and block size n assuming several well-known underlying distributions for the density of X , $f_X(\cdot)$. In some cases, the **EMR** (denoted $\bar{m} = \mathbb{E}[M]$) is also shown.

1. First, we consider the Gaussian distribution whose distribution function belongs to the **MDA** of the Gumbel distribution and serves as the limiting distribution in the **CLT**. Without loss of generality, let $X \sim N(0, \sigma^2)$, $f_X(x) = \frac{1}{\sigma\sqrt{2\pi}} \exp\left(-\frac{x^2}{2\sigma^2}\right)$, $\sigma > 0$. From Eqs. (1) and (3) we have,

$$f_M(m) = \frac{n \exp\left(-\frac{m^2}{2\sigma^2}\right) \left(1 - \frac{1}{2} \operatorname{erfc}\left(\frac{m}{\sigma\sqrt{2}}\right)\right)^{n-1}}{\sigma\sqrt{2\pi}}$$
$$F_M^{-1}(u) = \sigma\sqrt{2} \operatorname{erfc}^{-1}\left(2 - 2u^{1/n}\right)$$
$$m^* \approx \sigma \sqrt{W_0\left(\frac{n^2}{2\pi}\right)}$$

$$F_M(m^*) = \left(1 - \frac{1}{2} \operatorname{erfc} \left(\sqrt{\frac{W_0 \left(\frac{n^2}{2\pi} \right)}{2}} \right) \right)^n \approx \exp(-1)$$

where $\operatorname{erfc}(\cdot)$ is the complementary error function, $\operatorname{erfc}^{-1}(\cdot)$ is the inverse complementary error function, and $W_0(\cdot)$ is the principal branch of the product logarithm or Lambert W function (Johansson, 2020), which gives the root of $x \exp(x) - y = 0$. Notice $\frac{\partial m^*}{\partial \log(n)} = \frac{\sigma \sqrt{W_0 \left(\frac{n^2}{2\pi} \right)}}{1 + W_0 \left(\frac{n^2}{2\pi} \right)} \rightarrow 0$ as $n \rightarrow \infty$, MPMR arising from a Gaussian scales up slowly w.r.t. n , after a sufficiently large n .

- Given $Y \sim N(0, \sigma^2)$, we have $X = |Y| \sim HN\left(\frac{1}{\sigma}\sqrt{\frac{\pi}{2}}\right)$ as a random variable following half Normal distribution, whose distribution function belongs to the MDA of Gumbel, with $f_X(x) = \frac{1}{\sigma}\sqrt{\frac{2}{\pi}}\exp\left(-\frac{x^2}{2\sigma^2}\right)$, $\sigma > 0$, $x > 0$. From Eqs. (1) and (3) we have,

$$\begin{aligned} f_M(m) &= \sqrt{\frac{2}{\pi}} \frac{n}{\sigma} \exp\left(-\frac{m^2}{2\sigma^2}\right) \operatorname{erf}\left(\frac{m}{\sqrt{2}\sigma}\right)^{n-1} \\ F_M^{-1}(u) &= \sigma\sqrt{2} \operatorname{erf}^{-1}\left(u^{1/n}\right) \\ m^* &\approx \sigma\sqrt{W_0\left(\frac{2n^2}{\pi}\right)} \\ F_M(m^*) &= \operatorname{erf}\left(\frac{W_0\left(\frac{2n^2}{\pi}\right)}{2}\right)^n \approx \exp(-1) \end{aligned}$$

where $\operatorname{erf}(\cdot)$ is the Gauss error function, and $\operatorname{erf}^{-1}(\cdot)$ is the inverse Gauss error function.

- Next, we consider the GPD, whose distribution function belongs to the MDA of Frechet ($\xi > 0$) and serves as the limiting distribution in the Pickands-Balkema-de Haan theorem. Without loss of generality, let $X \sim GPD\left(\frac{1}{\xi}, 1, \xi\right)$, which follows Pareto Type I (power-law) distribution with scale $\frac{1}{\xi}$ and shape $\frac{1}{\xi}$, $f_X(x) = (\xi x)^{-\frac{\xi+1}{\xi}}$, $\xi > 0$, $x > \frac{1}{\xi}$. From Eqs. (1) and (2) we have,

$$\begin{aligned} f_M(m) &= n (\xi s)^{-\frac{n+\xi}{\xi}} \left((\xi s)^{1/\xi} - 1 \right)^{n-1} \\ F_M^{-1}(u) &= \frac{(1 - u^{1/n})^{-\xi}}{\xi} \end{aligned}$$

$$m^* = \frac{\left(\frac{n+\xi}{\xi+1}\right)^\xi}{\xi} \approx \frac{\left(\frac{n}{\xi+1}\right)^\xi}{\xi}$$

$$F_M(m^*) = \left(\frac{n-1}{n+\xi}\right)^n \approx \exp(-1-\xi)$$

When $k < \frac{1}{\xi}$, using Euler's reflection formula and the reciprocal gamma function (Olver et al.), with n and k as positive integers, the k -th raw moment of the BM is:

$$\begin{aligned} \mathbb{E}[M^k] &= -(1/\xi)^k \frac{\mathcal{B}(n, 1-n)}{\mathcal{B}(-n, n+1-k\xi)} \\ &= n \xi^{-k} \mathcal{B}(n, 1-k\xi), \quad k < \frac{1}{\xi} \\ \bar{m} &= \frac{n}{\xi} \mathcal{B}(n, 1-\xi), \quad \xi < 1 \\ \mathbb{V}[M] &= \frac{n(\mathcal{B}(n, 1-2\xi) - n\mathcal{B}(n, 1-\xi)^2)}{\xi^2}, \quad \xi < \frac{1}{2} \end{aligned}$$

where $\mathcal{B}(\cdot, \cdot)$ is the beta function. When $\xi < \frac{1}{2}$, the variance of BM exists but increases with n , leading to a wider spread of the BM distribution as n becomes larger.

4. The last distribution we consider is the exponential, $X \sim GPD(0, \xi, 0)$ whose distribution function belongs to the MDA of Gumbel distribution, with $f_X(x) = \frac{\exp(-\frac{x}{\xi})}{\xi}$, $\xi > 0, x > 0$. The exponential distribution can also be obtained by taking $X = \log(\xi Y) \sim Exp(\frac{1}{\xi})$, with $Y \sim GPD(\frac{1}{\xi}, 1, \xi)$ (Y follows Pareto Type I distribution). From Eqs. (1) and (2) we have,

$$f_M(m) = \frac{n \exp(-\frac{s}{\xi}) \left(1 - \exp(-\frac{s}{\xi})\right)^{n-1}}{\xi}$$

$$F_M^{-1}(u) = -\xi \log\left(1 - u^{1/n}\right)$$

$$m^* = \xi \log(n) \tag{A1}$$

$$\mathcal{M}_M(t) = n \mathcal{B}(n, 1-t\xi)$$

$$\bar{m} = \xi \sum_{i=1}^n \frac{1}{i} \approx \xi(\gamma + \log(n) + \frac{1}{2n}) \tag{A2}$$

$$\mathbb{V}[M] = \frac{\xi^2}{6} \left(\pi^2 - 6\psi^{(1)}(n+1)\right) \approx \frac{\xi^2 \pi^2}{6} \tag{A3}$$

$$F_M\left(m^* + k \frac{\xi\pi}{\sqrt{6}}\right) \approx F_M\left(\bar{m} + k \frac{\xi\pi}{\sqrt{6}}\right)$$

$$\approx \left(1 - \frac{\exp\left(-\frac{k\pi}{\sqrt{6}}\right)}{n} \right)^n \quad (\text{A4})$$

where $\mathcal{M}_M(\cdot)$ is the moment generating function of **BM**. The **EMR** \bar{m} has a harmonic number term and γ is the Euler's constant. The variance of the **BM** involves the trigamma function $\psi^{(1)}(z) := \frac{d^2}{dz^2} \log \Gamma(z)$.

References

- Aliyari Ghassabeh, Y.: On the convergence of the mean shift algorithm in the one-dimensional space. *Pattern Recognition Letters* **34**(12), 1423–1427 (2013) <https://doi.org/10.1016/j.patrec.2013.05.004>
- Berghaus, B., Bücher, A.: Weak convergence of a pseudo maximum likelihood estimator for the extremal index. *The Annals of Statistics* **46**(5), 2307–2335 (2018) <https://doi.org/10.1214/17-AOS1621>
- Belzile, L.R., Dutang, C., Northrop, P.J., Opitz, T.: A modeler's guide to extreme value software. *Extremes* **26**(4), 595–638 (2023) <https://doi.org/10.1007/s10687-023-00475-9>
- Bouchaud, J.-P., Potters, M.: *Theory of Financial Risk and Derivative Pricing: from Statistical Physics to Risk Management*, 2nd edn. Cambridge University Press, Cambridge (2003). <https://doi.org/10.1017/CBO9780511753893>
- Chen, K., Cheng, T.: Measuring tail risks. *The Journal of Finance and Data Science* **8**, 296–308 (2022) <https://doi.org/10.1016/j.jfds.2022.11.001>
- Clarkson, D., Eastoe, E., Leeson, A.: The importance of context in extreme value analysis with application to extreme temperatures in the u.s. and greenland. *Journal of the Royal Statistical Society Series C: Applied Statistics* **72**(4), 829–843 (2023) <https://doi.org/10.1093/jrssc/qlad020>
- Cheng, Y.: Mean shift, mode seeking, and clustering. *IEEE Transactions on Pattern Analysis and Machine Intelligence* **17**(8), 790–799 (1995) <https://doi.org/10.1109/34.400568>
- Chernick, M.R., NetLibrary, I.: *Bootstrap Methods: a Guide for Practitioners and Researchers*, 2nd edn. Wiley-Interscience, Hoboken, N.J (2008). <https://doi.org/10.1002/9780470192573>
- Clauset, A., Shalizi, C.R., Newman, M.E.J.: Power-law distributions in empirical data. *SIAM Review* **51**(4), 661–703 (2009) <https://doi.org/10.1137/070710111>
- Area Leão Pereira, E.J., Silva, M.F., Pereira, H.B.B.: Econophysics: Past and present. *Physica A: Statistical Mechanics and its Applications* **473**, 251–261 (2017) <https://doi.org/10.1016/j.physa.2017.04.038>

[//doi.org/10.1016/j.physa.2017.01.007](https://doi.org/10.1016/j.physa.2017.01.007)

- Davison, A.C., Huser, R.: Statistics of extremes. *Annual Review of Statistics and Its Application* **2**, 203–235 (2015) <https://doi.org/10.1146/annurev-statistics-010814-020133>
- Haan, L., Tank, A.K., Neves, C.: On tail trend detection: modeling relative risk. *Extremes* **18**(2), 141–178 (2015) <https://doi.org/10.1007/s10687-014-0207-8>
- Estilow, T.W., Young, A.H., Robinson, D.A.: A long-term northern hemisphere snow cover extent data record for climate studies and monitoring. *Earth System Science Data* **7**(1), 137–142 (2015) <https://doi.org/10.5194/essd-7-137-2015> . Publisher: Copernicus GmbH. Accessed 2024-04-10
- Ferreira, A., Haan, L.: On the block maxima method in extreme value theory: PWM estimators. *The Annals of Statistics* **43**(1), 276–298 (2015) <https://doi.org/10.1214/14-AOS1280>
- Fedotenkov, I.: A review of more than one hundred pareto-tail index estimators. *Statistica* **80**(3), 245–299 (2020) <https://doi.org/10.6092/issn.1973-2201/9533>
- Ferreira, M.: Extremal index: estimation and resampling. *Computational Statistics* (2023) <https://doi.org/10.1007/s00180-023-01406-9>
- Fetterer, F., Knowles, K., Meier, W., Savoie, M., Windnagel, A.: Sea Ice Index, Version 3. National Snow and Ice Data Center (2017). <https://doi.org/10.7265/N5K072F8>
- Gabaix, X.: Power laws in economics and finance. *Annual Review of Economics* **1**, 255–294 (2009) <https://doi.org/10.1146/annurev.economics.050708.142940>
- Gabaix, X.: Power laws in economics: An introduction. *Journal of Economic Perspectives* **30**(1), 185–206 (2016) <https://doi.org/10.1257/jep.30.1.185>
- Gattacceca, J., McCubbin, F.M., Grossman, J.N., Schrader, D.L., Chabot, N.L., D’Orazio, M., Goodrich, C., Greshake, A., Gross, J., Joy, K.H., Komatsu, M., Miao, B.: The meteoritical bulletin, no. 111. *Meteoritics & Planetary Science* **58**(6), 901–904 (2023) <https://doi.org/10.1111/maps.13995> . Accessed 2024-04-09
- Greenspan, A.: We will never have a perfect model of risk. *Financial Times* **16**(3) (2008). Accessed 2024-04-10
- Hill, B.M.: A simple general approach to inference about the tail of a distribution. *The Annals of Statistics* **3**(5), 1163–1174 (1975) <https://doi.org/10.1214/aos/1176343247>
- Huser, R., Wadsworth, J.L.: Advances in statistical modeling of spatial extremes. *Wiley Interdisciplinary Reviews: Computational Statistics* **14**(1), 1537 (2022) <https://doi.org/10.1002/wics.1537>

- Jochem Oorschot, Johan Segers, Chen Zhou: Tail inference using extreme u-statistics. *Electronic Journal of Statistics* **17**(1), 1113–1159 (2023) <https://doi.org/10.1214/23-EJS2129>
- Johansson, F.: Computing the lambert w function in arbitrary-precision complex interval arithmetic. *Numerical Algorithms* **83**(1), 221–242 (2020) <https://doi.org/10.1007/s11075-019-00678-x>
- Kratz, M.: On the estimation of the distribution of aggregated heavy-tailed risks: Application to risk measures. In: *Extreme Events in Finance*, pp. 239–282 (2016). <https://doi.org/10.1002/9781118650318.ch11>
- Leadbetter, M.R., Lindgren, G., Rootzén, H., SpringerLink (Online service): *Extremes and Related Properties of Random Sequences and Processes* vol. Book, Whole. Springer, New York, NY (1983). <https://doi.org/10.1007/978-1-4612-5449-2>
- Longin, F.M.: *Extreme Events in Finance: a Handbook of Extreme Value Theory and Its Applications* vol. Book, Whole, 1st edn. Wiley, Hoboken (2016). <https://doi.org/10.1002/9781118650318>
- McElreath, R.: *Statistical Rethinking: a Bayesian Course with Examples in R and Stan* vol. Book, Whole, 2nd edn. CRC Press, Boca Raton, FL (2020). <https://doi.org/10.1201/9780429029608>
- Moloney, N.R., Faranda, D., Sato, Y.: An overview of the extremal index. *Chaos: An Interdisciplinary Journal of Nonlinear Science* **29**(2), 022101 (2019) <https://doi.org/10.1063/1.5079656>
- Meerschaert, M.M., Scheffler, H.-P.: A simple robust estimation method for the thickness of heavy tails. *Journal of Statistical Planning and Inference* **71**(1-2), 19–34 (1998) [https://doi.org/10.1016/S0378-3758\(98\)00093-7](https://doi.org/10.1016/S0378-3758(98)00093-7)
- Nadarajah, S.: Saralees nadarajah’s contribution to the discussion of ‘the first discussion meeting on statistical aspects of climate change’. *Journal of the Royal Statistical Society Series C: Applied Statistics* **72**(4), 860–861 (2023) <https://doi.org/10.1093/jrsssc/qlad053>
- Northrop, P.J.: An efficient semiparametric maxima estimator of the extremal index. *Extremes* **18**(4), 585–603 (2015) <https://doi.org/10.1007/s10687-015-0221-5>
- Nolde, N., Zhou, C.: Extreme value analysis for financial risk management. *Annual Review of Statistics and Its Application* **8**, 217–240 (2021) <https://doi.org/10.1146/annurev-statistics-042720-015705>
- Nadarajah, S., Zhang, Y., Pogány, T.K.: On sums of independent generalized pareto random variables with applications to insurance and cat-bonds. *Probability in the Engineering and Informational Sciences* **32**(2), 296–305 (2018) <https://doi.org/10.1080/10989185.2018.1512345>

1017/S0269964817000055

- Olver, F.W.J., Olde Daalhuis, A.B., Lozier, D.W., Schneider, B.I., Boisvert, R.F., Clark, C.W., Miller, B.R., Saunders, B.V., Cohl, H.S., McClain, M.A.: NIST digital library of mathematical functions. <https://dlmf.nist.gov/>, Release 1.2.1 of 2024-06-15. F. W. J. Olver, A. B. Olde Daalhuis, D. W. Lozier, B. I. Schneider, R. F. Boisvert, C. W. Clark, B. R. Miller, B. V. Saunders, H. S. Cohl, and M. A. McClain, eds. <https://dlmf.nist.gov/>
- Oliveira, I.F.D., Takahashi, R.H.C.: An enhancement of the bisection method average performance preserving minmax optimality. *ACM Trans. Math. Softw.* **47**(1) (2020) <https://doi.org/10.1145/3423597>
- Politis, D.N., Romano, J.P., Wolf, M.: Subsampling. Springer series in statistics, pp. 253–269. Springer, New York (1999). <https://doi.org/10.1007/978-1-4612-1554-7>
- Qu, T., Mei, K.W., Doray, A.: A simple method to detect extreme events from financial time series data. *Machine Learning with Applications* **10**, 100415 (2022) <https://doi.org/10.1016/j.mlwa.2022.100415>
- SILSO World Data Center: The international sunspot number. International Sunspot Number Monthly Bulletin and online catalogue (1849-2024)
- Smith, A.B., Katz, R.W.: US billion-dollar weather and climate disasters: data sources, trends, accuracy and biases. *Natural Hazards* **67**(2), 387–410 (2013) <https://doi.org/10.1007/s11069-013-0566-5>
- Smith, R.L.: Estimating tails of probability distributions. *The annals of Statistics*, 1174–1207 (1987) <https://doi.org/10.1214/aos/1176350499>
- Smolka, A.: Natural disasters and the challenge of extreme events: risk management from an insurance perspective. *Philosophical Transactions of the Royal Society A: Mathematical, Physical and Engineering Sciences* **364**(1845), 2147–2165 (2006) <https://doi.org/10.1098/rsta.2006.1818>
- Sohkanen, P.: Estimation of the tail dependence coefficient (2021). Accessed 2024-04-10
- Schultze, J., Steinebach, J.: On least squares estimates of an exponential tail coefficient. *Statistics & Risk Modeling* **14**(4), 353–372 (1996) <https://doi.org/10.1524/strm.1996.14.4.353>
- Shindell, D.T., Schmidt, G.A., Mann, M.E., Rind, D., Waple, A.: Solar forcing of regional climate change during the maunder minimum. *Science* **294**(5549), 2149–2152 (2001) <https://doi.org/10.1126/science.1064363>
- Tao, T.: E pluribus unum: From complexity, universality. *Daedalus* **141**(3), 23–34

(2012) https://doi.org/10.1162/DAED_a_00158

US Geological Survey, E.H.P.: Advanced national seismic system (ANSS) comprehensive catalog of earthquake events and products: Various (2017). Accessed 2024-04-09

Wager, S.: Subsampling extremes: From block maxima to smooth tail estimation. *Journal of Multivariate Analysis* **130**, 335–353 (2014) <https://doi.org/10.1016/j.jmva.2014.06.010>

Welford, B.P.: Note on a method for calculating corrected sums of squares and products. *Technometrics* **4**(3), 419–420 (1962) <https://doi.org/10.1080/00401706.1962.10490022>

Zwiers, F.W., Alexander, L.V., Hegerl, G.C., Knutson, T.R., Kossin, J.P., Naveau, P., Nicholls, N., Schär, C., Seneviratne, S.I., Zhang, X.: Climate extremes: Challenges in estimating and understanding recent changes in the frequency and intensity of extreme climate and weather events. In: Asrar, G.R., Hurrell, J.W. (eds.) *Climate Science for Serving Society: Research, Modeling and Prediction Priorities*, pp. 339–389. Springer, Dordrecht (2013). https://doi.org/10.1007/978-94-007-6692-1_13